Petrography, geochemistry and stable isotopes of carbonate rocks, Lower Cretaceous Alisitos Formation, Los Torotes section, Baja California, Mexico

Jayagopal Madhavaraju[1*], Hannes Löser[1], Robert W. Scott[2], Satheesan Sandeep[3], Alcides N. Sial[4], and Sooriamuthu Ramasamy[3]

[1] Estación Regional del Noroeste, Instituto de Geología, Universidad Nacional Autónoma de México, Hermosillo, Sonora, 83000, Mexico.
[2] Precision Stratigraphy Associates & The University of Tulsa, 149 West Ridge Road, Cleveland Oklahoma, 74020, USA.
[3] Department of Geology, University of Madras, Chennai 600 025, India.
[4] Nucleo de Estudos Geoquímicos e Laboratório de Isótopos Estáveis (NEG - LABISE) Departmento de Geologia, Universidade Federal de Pernambuco, Caixa Posta, 7852, 50670-000 Recife, PE, Brazil.
** mj@geologia.unam.mx*

ABSTRACT

Petrography, stable carbon and oxygen isotopes, and major, trace, and rare earth elements geochemistry of limestones of the Alisitos Formation in the Los Torotes, Baja California were studied in order to document the elemental variations among Member C (MC) and Member E (ME) of the formation and to understand their diagenetic and depositional conditions. The major petrographic types identified are mudstone, wackestone and packstone. The limestones of the Alisitos Formation show significant variations in $\delta^{13}C$ and $\delta^{18}O$ values (+4.13 to +5.26‰; -14.17 to -6.84‰; respectively). The limestones from Member C (MC) show higher ΣREE content (23 ± 17, n=10) than Member E (ME) (11 ± 5.5, n=9) of the Alisitos Formation. The observed variations in ΣREE content in these limestones are due to the amount of detrital material present in them. The limestones from ME record seawater-like REE+Y patterns, whereas the MC records non-seawater-like signatures (*i.e.* significant enrichment of middle rare earth elements: MREE). Most of the analyzed samples from the Alisitos Formation show negative Ce anomalies (Ce/Ce*: 0.67 – 0.99, n=17). The limestones show both negative and positive Eu anomalies (Eu/Eu*: 0.58 – 2.91, n=19). The positive Eu anomalies identified in many samples may be due to the influence of hydrothermal fluids or co-precipitation of hydrothermal Fe-sulfide. The limestones of ME exhibit seawater-like-REE patterns suggesting that most of the REEs present in them were derived from seawater. However, the limestones of MC were contaminated by detrital materials which effectively mask the seawater-like signatures. The detrital materials present in the limestones of MC were probably derived from the mafic to felsic source rocks.

Key words: Geochemistry; stable isotopes; carbonate rocks; Baja California; Mexico.

RESUMEN

La petrografía, composiciones isotópicas (carbono y oxígeno) y geoquímicas (elementos mayores, traza y de tierras raras en calizas de la Formación Alisitos en el área Los Torotes, Baja California fueron estudiadas con el fin de documentar las variaciones elementales entre el Miembro C (MC) y el Miembro E (ME) con la finalidad de entender las condiciones diagenéticas y depositacionales. Los principales tipos petrográficos identificados fueron mudstone, wackestone y packstone. Las calizas de la Formación Alisitos muestran notables variaciones en $\delta^{13}C$ y $\delta^{18}O$ (+4.13 a +5.26‰; -14.17 a -6.84‰; respectivamente). Las calizas del Miembro C (MC) muestran contenidos más altos de elementos tierra raras totales (ΣREE por su siglas en inglés) (23 ± 17, n=10) que las del Miembro E (ME) (11 ± 5.5, n=9) en la Formación Alisitos. Las variaciones observadas en los contenidos de tierras raras totales en esas calizas son debido a la cantidad de material detrítico presente en ellas. Las calizas de ME registran patrones REE+Y similares a las aguas marinas, mientras MC registra firmas distintas a las aguas marinas, es decir, tienen un significante enriquecimiento de tierra raras medias. La mayoría de las muestras analizadas de la Formación Alisitos señalan anomalías negativas de Ce (Ce/Ce: 0.67 – 0.99, n=17). Las calizas estudiadas muestran tanto anomalía positiva como negativa de Eu (Eu/Eu*: 0.58 – 2.91, n=19). Las anomalías positivas de Eu identificadas en muchas muestras podrían deberse a la influencia de fluidos hidrotermales o a la co-precipitación de sulfuro de Fe hidrotermal. Las calizas de ME exhiben patrones de REE similares a las aguas marinas lo que sugiere que las mayoría de REE presentes en estas calizas son derivadas de aguas marinas. Sin embargo, las calizas de MC fueron contaminadas por materiales detríticos los cuales ocultan efectivamente las firmas similares a las aguas marinas. El material detrítico presente en las calizas de MC se derivó probablemente de rocas fuentes máficas a félsicas.*

Palabras clave: Geoquímica; isótopos estables; rocas carbonatadas; Baja California; México.

INTRODUCTION

Rare earth element concentrations (REEs) in seawater are primarily influenced by different sources (*e.g.* terrestrial input from continental weathering and sea-floor hydrothermal vents) and scavenging processes related to depth, salinity and oxygen levels (Elderfield, 1988; Greaves *et al.*, 1999). REE chemistry is a valuable tool for investigating

Madhavaraju, J., Löser, H., Scott, R.W., Sandeep, S., Sial, A.N., Ramasamy, S., 2017, Petrography, geochemistry and stable isotopes of carbonate rocks, Lower Cretaceous Alisitos Formation, Los Torotes section, Baja California, Mexico: Revista Mexicana de Ciencias Geológicas, v. 34 núm. 2, p. 63-77.

palaeoenvironments because the relative abundances of REE in hydrogenous sediments (*i.e.* autochthonous sediments deposited in basin waters) such as carbonate and chert, vary systematically depending on the influence of hydrothermal, terrestrial or marine inputs upon fluids in the basin (Van Kranendonk *et al.*, 2003).

Marine chemical sediments mainly exhibit seawater-like REE+Y patterns that appear to be irrespective of geological ages (Shields and Webb, 2004; Bolhar and Van Kranendonk, 2007). Post Archean Australian Shale (PAAS) normalized seawater REE patterns exhibit uniform light rare earth elements (LREE) depletion, negative Ce anomaly, positive La anomaly and high Y/Ho ratios (*e.g.* De Baar *et al.*, 1991; Bau and Dulski, 1996: Nagarajan *et al.*, 2011; Madhavaraju and González-León, 2012) are differentiated from detrital input (flat pattern) and hydrothermal input (positive Eu anomaly, enriched LREE and MREE). Hydrothermal fluids mainly display REE+Y patterns with positive Eu anomaly and light to middle REE-enriched patterns when normalized to PAAS (Wheat *et al.*, 2002). However, river water shows flat REE+Y patterns with slight light REE depletion and no anomalies and so marine and lacustrine carbonates can be easily distinguished (Bolhar and Van Kranendonk, 2007; Garcia *et al.*, 2007). In ancient carbonate rocks, REEs provide important information regarding the marine and estuarine redox history (German and Elderfield, 1990; Bellanca *et al.*, 1997) and palaeoceanography (Liu, *et al.*, 1988; Shields and Webb, 2004). Nothdurft *et al.* (2004) distinguished REE patterns in microbialites that formed in estuarine fringing reefs versus offshore and more open marine settings.

The carbon and oxygen isotopic compositions, along with petrography of carbonate rocks, may prove to be powerful tools to trace fluid origin and to reconstruct large-scale movements and evolution of fluids (Allan and Matthews, 1982). The diagenesis of carbonate rocks includes all the processes that affect the sediments after deposition and up to the processes of metamorphism at high temperatures and pressures (Moore, 2001). Carbonate rocks deposited in marine environments mainly preserve the carbon isotopic composition of the ocean water (Scholle and Arthur, 1980). The stratigraphic correlation of marine carbonates by means of carbon isotope data has been applied to Cretaceous marine carbonate sediments (Jenkyns, 1995; Weissert *et al.*, 1998; Moullade *et al.*, 1998; Grotsch *et al.*, 1998; Armstrong-Altrin *et al.*, 2011; Madhavaraju *et al.*, 2013a, 2013b).

The Aptian-Albian Alisitos Formation is exposed across the western half of northern Baja California as a discontinuous belt 600 km long that trends parallel to the Pacific coast and is approximately 50 km wide. The Alisitos Formation exposed between Ensenada and La Bocana along the Baja California Peninsula has attracted the attention of many researchers for its extensive volcaniclastic strata (Tardy *et al.*, 1993; Morán-Zenteno, 1994) and thick fossiliferous limestones (Allison, 1955, 1974). The marine sediments occur throughout the Alisitos Formation, however, the thicker sequences are found in the lower part (Wetmore *et al.*, 2005). For the present study, limestone samples were collected from the well exposed section situated near Los Torotes (Almázan-Vázquez, 1988) (Figure 1). Stable isotope and geochemical (major, trace and REE) studies were undertaken on the limestones of the Alisitos Formation. The aims of the study are to document the influence of terrigenous materials on REE characteristics of carbonate rocks; to unravel the probable reason for significant variations in REE patterns; and to understand the diagenetic and depositional conditions in the limestones of the Alisitos Formation.

GEOLOGY AND STRATIGRAPHY

The Cretaceous Alisitos Formation forms part of the Guerrero terrane (Campa and Coney, 1983) and is exposed in the northern part of Baja California (Figure 1). The first detailed study on the volcanosedimentary sequences was carried out by Santillan and Barrera (1930) and they named these deposits the Alisitos Formation after the Alisitos Ranch in the Río Santo Tomás valley. The Alisitos Formation was derived from a volcanoplutonic arc developed along the western margin

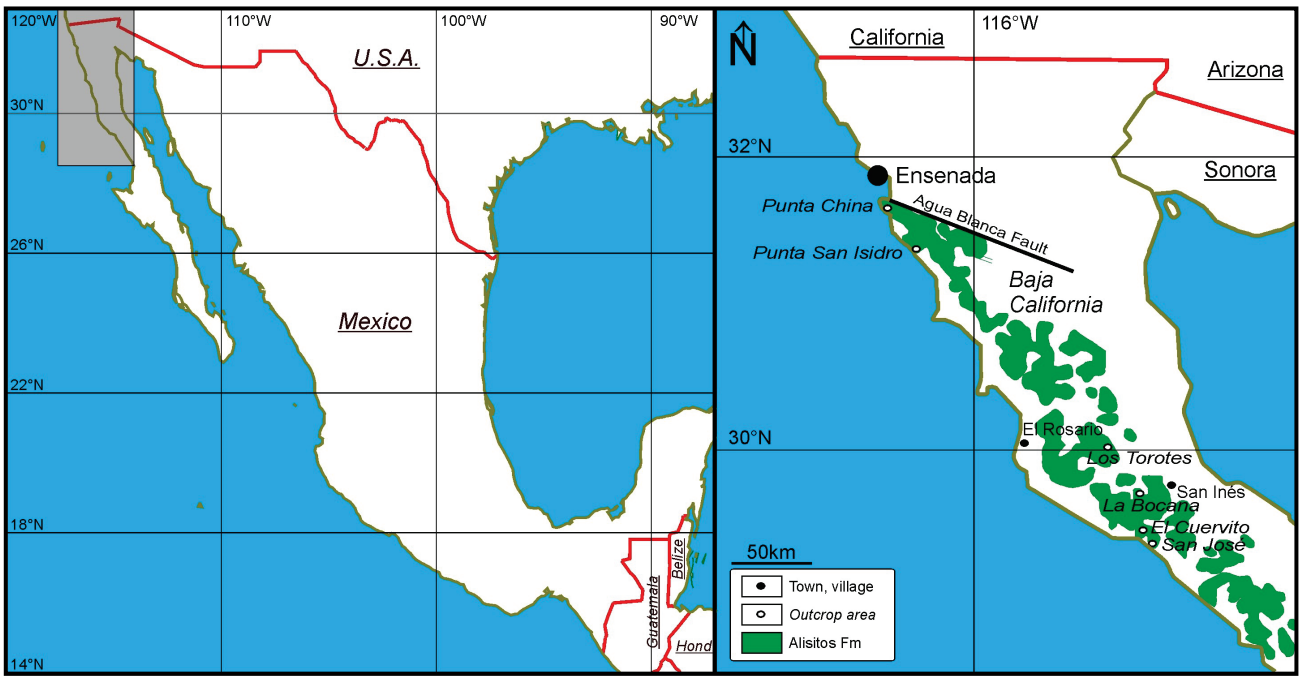

Figure 1. Location map of the Alisitos Formation in Los Torotes área (Los Torotes Section, Baja Ca, Mexico UTM : PP72. Latitude : 30.000, Longitude : -115.200; and Geographical coordinates in degrees minutes seconds (WGS84) Latitude : 30 00' 00" Longitude : -115 12' 00".

of Baja California during the Early Cretaceous (*ca*. 140–100 Ma; Busby 2004). The Alisitos Formation is estimated to be about 6,000 to 7,500 m thick and spans from at least Aptian to Albian in age (Allison, 1974; Wetmore *et al.*, 2005).

The Los Torotes section between El Rosario and San Inés and the La Bocana section about 12 km northwest of San Inés were studied by Almazán-Vázquez and Buitrón-Sánchez (1984) and Almázan-Vázquez (1988). Paleontology, petrography and lithologic associations enable chronstatigraphic correlation between Los Torotes and La Bocana (SW San Inés) and El Cuervita - San Jose areas, which have different sedimentologic characteristics. The Los Torotes and La Bocana sections have 5,000 m thick sequences and have been interpreted to be a deposit of insular arc margin, whereas El Cuervita - San Jose areas shows a clear contrast because the strata here are 1,500 m thick and represents sedimentation in an insular fore-arc basin. The Alisitos Formation was deformed by the Oregonian Orogeny during the late Albian, which produced disharmonic synclines and anticlines, subsequently basement folds with wide radius of curvature and, finally, origination of a northwest-southeast trending regional fault with lateral displacement.

Los Torotes section

The Alisitos Formation is well exposed in the north of Los Torotes ranch, where a 3,500 m thick volcano-sedimentary sequence was measured (Figure 2). The Los Torotes Section has received much attention by many studies in recent decades because of its sedimentological variations, richness of fossils and easy accessibility to carry out research activities. Beggs (1984) did the earliest systematic description, however, he described only a small portion of the section.

The Alisitos Formation exposed in the Los Torotes area has been divided into six distinct informal members, viz. member A, B, C, D, E and F (Almazan-Vazquez, 1988). Among them, the carbonate rocks are well exposed in members C and E. Member A consists of interbedded recrystallized limestone and volcaniclastic rocks. The limestone beds are gray, laminated lenticular beds 2 to 9 m thick. The limestone beds are recrystallized in several places. The volcanic rocks are yellow and light green with cryptocrystalline tuffs and volcanic breccias 10 to 25 m thick. Member B is mainly composed of pyroclastic rocks (tuffs and volcanic breccias) interbedded with epiclastic rocks (sandstone and siltstone). Member C mainly consists of limestone with epiclas-

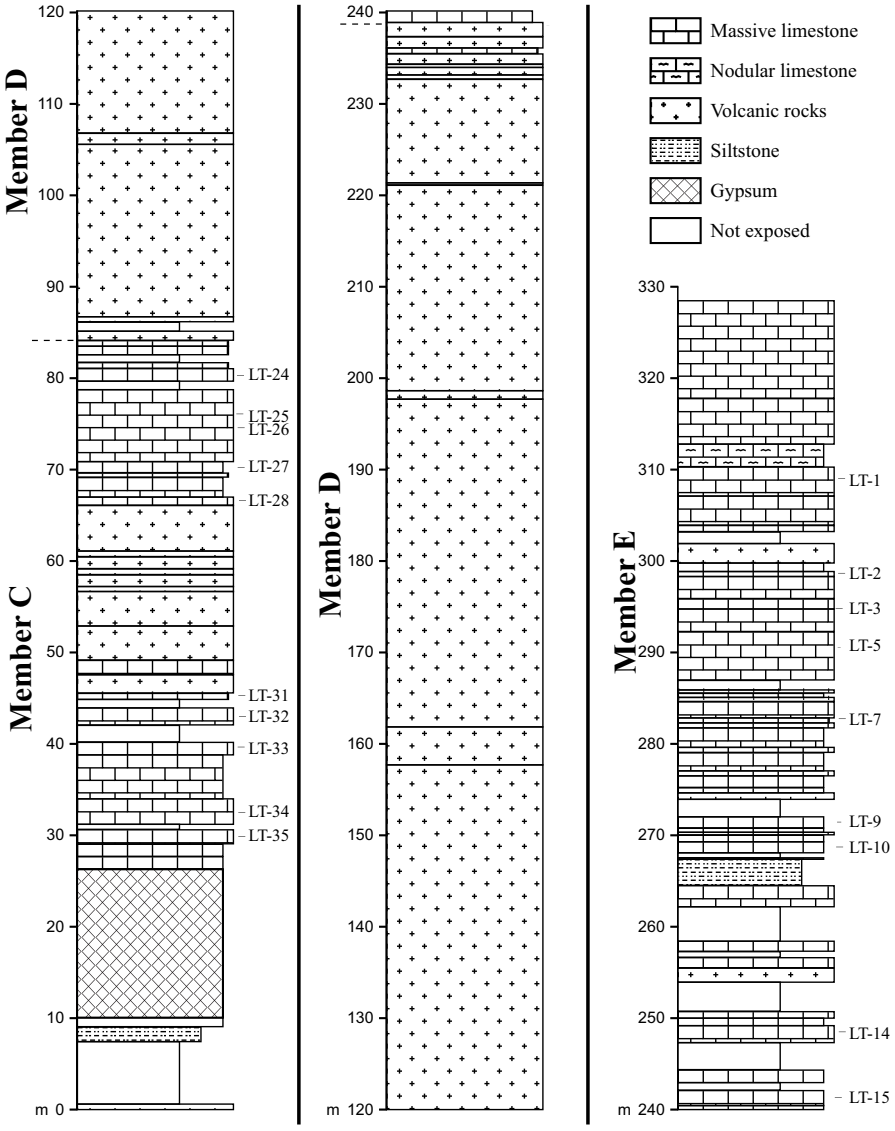

Figure 2. Lithostratigraphic section of the Alisitos Formation in Los Torotes area.

tic rocks. Member D is mainly composed of lavas interbedded with tuffs. Member E consists of biohermal limestone, epiclastic rocks and pyroclastic rocks. Member F is mainly composed of pyoclastic rocks up to 2,500 m thick.

A detailed lithostratigraphic description of the Alisitos Formation is given in Figure 2. Samples were collected from the Los Torotes section and the observed lithological units are given in the lithostratigraphic columns (Figure 2). The present study focuses on the carbonate rocks exposed in the Los Torotes section and an interval only 350 m thick that mainly consists of Member C, Member D and Member E is measured. The base of the measured section is in Member C (Almazan-Vazquez, 1988), where only limestones, gypsum, siltstone and pyroclastic rocks are exposed (Figure 3a), whereas softer sediments such as marls or clays are covered with soil. Member C is overlain by a thick sequence of pyroclastic rocks, which is correlated with Member D (MD). Above is Member E, which is mainly fossiliferous limestone, nodular limestone, siltstone and thin beds of pyroclastic rocks (Figure 3b).

Table 1. Comparison of major oxide data for ES-3 reference sample with certificate of analysis data as well as limits of detection (LOD) data for XRF analyses.

Oxide/ Elements	This study*	Literature value	LOD**
SiO_2	4.85	4.84	0.050
Al_2O_3	1.22	1.10	0.018
Fe_2O_3	0.60	0.61	0.006
CaO	50.28	50.50	0.040
MgO	0.79	0.85	0.015
K_2O	0.61	0.51	0.030
Na_2O	0.07	0.08	0.050
MnO	0.06	0.06	0.004
TiO_2	0.07	0.08	0.004
P_2O_5	0.43	0.42	0.004
LOI	–	–	–

* Major elements in wt % are by XRF; ** LOD (limit of detection) in wt%; – : not determined or not reported; LOI: Loss on ignition.

MATERIALS AND METHODS

Nineteen limestone samples from the Los Torotes section were selected for geochemical study (Figure 2) and these samples were powdered in an agate mortar. Major oxides composition was obtained by X-ray fluorescence in fused $LiBO_2/Li_2B_4O_7$ disks using an X-ray fluorescence spectrometer (Siemens SRS-3000) with an Rh-anode X-ray tube as a radiation source. X-ray absorption/enhancement effects were corrected using the Lachance and Traill (1966) method, included in the SRS-3000 software. One gram of sample was heated to 1,000 °C in porcelain crucibles for 1 hour to measure the Loss-on-Ignition (LOI). The geochemical standard ES-3 was used to determine data quality (Table 1). The analytical accuracy errors were better than ±2% for SiO_2, Fe_2O_3 and CaO, better than ±3% for MnO and P_2O_5 and better than ±7% for MgO. The accuracy errors were more than ±10% for Al_2O_3, Na_2O, K_2O and TiO_2.

Trace and rare earth elements were determined by an Agilent 7500 CE Inductively Coupled Plasma Mass Spectrometer (ICP-MS) according to standard analytical procedures suggested by Eggins *et al.* (1997). The geochemical standards JLS1 and IGLa-1 were used to monitor the analytical reproducibility. The analytical results of JLS1 and IGLa-1 are compared with published values (Govindaraju, 1994) to check the quality and accuracy of the analyses (Table 2). PAAS values were used for REE-normalized diagrams (Taylor and McLennan, 1985). Such normalization highlights the differences in abundance between detrial sources (shale contamination) and the residual inventory in seawater after modification in the marine environment and further removal by adsorption on surfaces of suspended and sinking particles. Using PAAS normalized values, the anomalies are expressed as Ce/Ce* = Ce/(2Pr-1Nd) and Pr/Pr* = Pr/(0.5Ce+0.5Nd) (Bau and Dulski, 1996; Bolhar *et al.*, 2004).

Nineteen limestone samples were selected for stable isotopic study. The carbon and oxygen isotope compositions were analyzed using an SIRA II mass spectrometer at the Stable Isotope Laboratory (LABISE) of the Federal University of Pernambuco, Brazil. The limestone samples were treated with H_3PO_4 in a vacuum at 25°C for one day for the determination of carbon and oxygen isotopes and the resulted CO_2 gas analyzed according to the method described by Craig (1957). CO_2 gas released by this method was analyzed in a double inlet, triple collector SIRA II mass spectrometer using the reference gas BSC (Borborema Skarn Calcite), which was calibrated against NBS-18, NBS-19, and NBS-20 and has a value of -11.28 ± 0.004 ‰ VPDB for $\delta^{18}O$ and -8.58 ± 0.02 ‰ VPDB for $\delta^{13}C$. The results reported in the notation δ‰ (per mil) in relation to international VPDB scale.

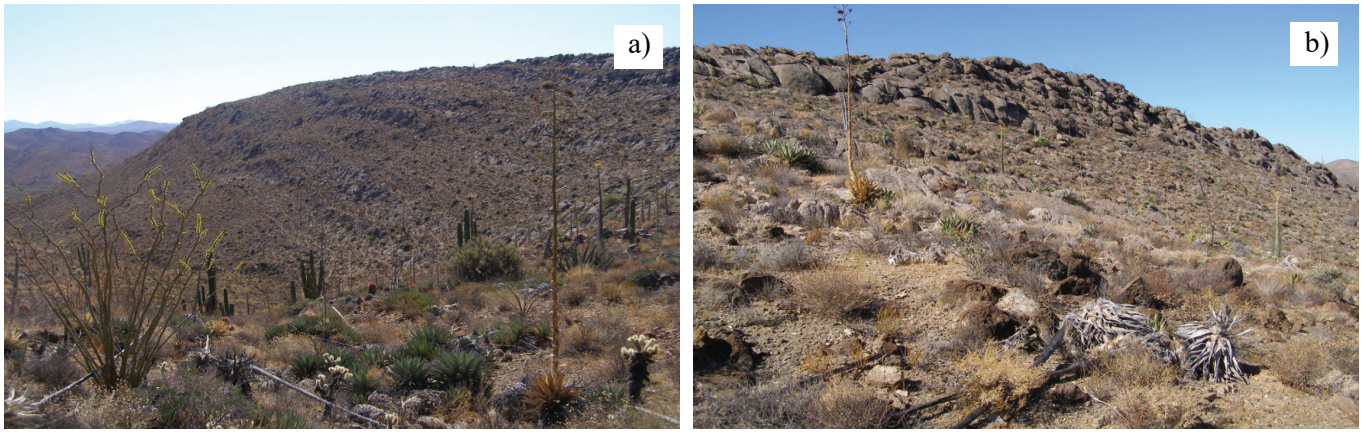

Figure 3. a) Panoramic view of Member C of the Los Torotes section of the Alisitos Formation and b) Fossiliferous limestone of Member E well exposed in the upper part of the Los Torotes section.

RESULTS

Lithofacies and diagenesis

Member C

Member C is composed of two intervals of limestone about 20 m thick each separated by volcanoclastic strata The interval from 29 m to 50 m is dominantly bedded rudist bioclastic packstone (thin sections LT35 - LT31; Figures 4a, 4b; Table 3). Bivalves including caprinid racists and other rudists and echinoderm closets are the principle carbonate grain types; coral fragments are in one sample. The uppermost two beds are unfossiliferous lime mudstone interbedded with volcanoclastic beds (Figure 4c). Non-carbonate grains are in trace amounts; at the base are lithoclasts and higher samples have quartz, feldspar, volcanoclasts (Figure 4d), and chert grains. The next higher interval of Member C from 67 to 83 m is composed of rudist bioclast packstone (Figures 4e, 4f) with echinoderm plates; one sample has the calcareous alga, *Cayeuxia* sp. (thin sections LT28 - LT24). The topmost sample is chondrodontid bioclastic packstone.

The micrite matrix was recrystallized in places and chondrodont shells were partly replaced by silica (Figure 4e). During burial some samples experienced compaction and stress (Figure 4b) followed by formation of thin wavy to irregular stylolites infused by opaque minerals (Figure 4b). The resolvable paragenetic succession is: 1) encrustation of bioclasts by cyanobacteria resulting in micritic films; 2) formation of opaque minerals; 3) recrystallization of micrite matrix; 4) chert partly replacing shells and locally matrix; 5) burial and formation of stylolites and calcite stress lineations; and 6) alteration of iron-bearing minerals.

Member E

Oyster bioclast packstone-wackestone comprises the interval from about 240 m to 322 m (Figure 5a).The lower three samples have

Table 2. Comparison of data of trace and rare earth elements for IGLa-1 and JLs-1 reference samples.

Oxide/ Elements	IGLa-1	JLs-1	This study*		LOD **
			IGLa-1	JLs-1	
Ba	918.50	476.00	897.00	469.00	2.9712
Co	11.29	0.08	11.57	0.21	0.0213
Cr	29.21	3.37	29.91	3.80	2.4233
Sc	12.19	0.03	13.29	–	0.0472
V	97.97	3.59	95.14	3.52	1.3595
Y	27.25	0.22	28.38	0.33	0.1902
Sr	574.70	295.00	531.00	297.00	6.0714
Zr	241.90	4.19	247.00	4.15	4.3175
Nb	18.96	1.00	19.30	–	0.0102
Ni	8.38	0.36	8.74	–	0.5802
Pb	10.24	0.70	11.09	–	0.3249
Rb	32.77	0.18	33.75	0.19	0.4833
Th	2.97	0.03	2.97	0.02	0.0151
U	0.99	1.75	1.06	1.70	0.0217
La	28.96	0.153	29.36	0.12	0.0136
Ce	56.73	0.521	54.56	0.50	0.0351
Pr	7.13	0.032	7.15	0.06	0.0088
Nd	28.65	0.136	29.25	0.22	0.0107
Sm	6.13	0.135	6.16	0.05	0.0918
Eu	1.85	0.007	1.84	–	0.0435
Gd	5.96	0.03	5.98	0.03	0.0028
Tb	0.88	0.004	0.89	0.005	0.0535
Dy	4.87	0.028	4.93	0.03	0.1087
Ho	0.99	–	0.99	0.01	0.0070
Er	2.76	–	2.62	0.02	0.0360
Tm	0.39	–	0.41	0.01	0.0071
Yb	2.60	0.016	2.60	0.03	0.0605
Lu	0.41	0.022	0.39	0.02	0.0077

* Trace and rare earth elements in ppm by ICP-MS. ** LOD (limit of detection) in ppb; – : not determined or not reported.

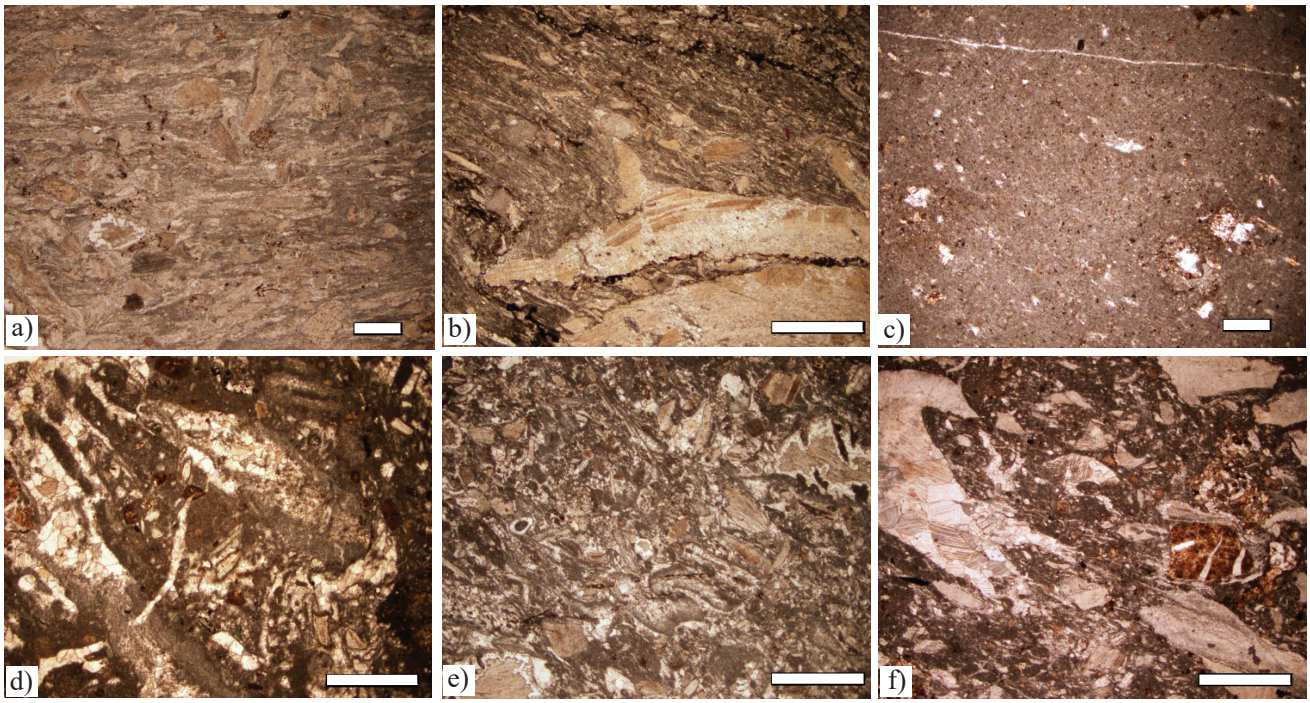

Figure 4. a) Bioclastic packstone, LT-32. b) Caprinid bioclastic packstone with calcite lineations, LT-34, c) Lime mudstone with incipient stylolites, LT-31. d) Bioclastic packstone, rudist and coral bioclasts, LT-33. e) Bioclastic packstone with chondrodontid clasts and chert rims partly replace bioclasts, LT-24, f) Volcanoclastic rudist-peloid bioclastic packstone, LT-28. Scale bar for figures c, e = 250 µm; scale bar for figures a, b, d, f= 500 µm.

Table 3.Petrography of Alisitos Formation, Los Torotes Section - Baja California (in stratigraphic order; wkst: wackestone, pkst: packstone, dolo: , qtz quartz, feld: feldspar).

	Facies	Number of Taxa	Bivalves	Rudists	Caprinids	Monopleurids/ Radiolitids	Chondrodonta	Echinoderm	Cayeuxia piae	Lithocodium aggregatum	Coral	Non-biotic components			
Member E	*Volcanoclastic Interval*														
	LT1 Bioclastic Pkst, dolo	5	X	X			X	X		X		leucoxene	chert	microspar	
	LT2 Bioclastic Wkst, dolo	3	X					X	X			leucoxene	c hert	microspar	Stress lineation
	LT3 Bioclastic Wkst, dolo	2	X					X				leucoxene	chert	microspar	
	LT9 Bioclastic Wkst	2	X					X				leucoxene	chert	microspar	
	LT14 Bioclastic Pkst	1	X									leucoxene	chert	microspar	Stress lineation
	LT15 Bioclastic Pkst	1	X									hematite		microspar	Stress lineation
	LT18 Bioclastic Wkst	1	X									pyrite	chert	microspar	
Member C	*Volcanoclastic Interval*														
	LT24 Bioclastic Pkst	3	X				X	X					chert		
	LT26 Bioclastic Pkst	3	X	X				X							
	LT25 Bioclastic Pkst	5	X	X		X		X	X						
	LT27 Bioclastic Pkst	3	X	X				X				feldspar	chert	microspar	Stress lineation
	LT28 Bioclastic Pkst-peloids	3	X	X				X				Volcanics	chert		
	Gypsum Interval														
	LT31 Lime Mudstone	0										qtz, feld			
	LT32 Bioclastic Pkst	3	X	X				X				qtz, feld	chert grains		
	LT33 Bioclastic Pkst	5	X	X	?			X			X	Volcanics			
	LT34 Bioclastic Pkst	3	X		X			X				qtz grains	chert		Stress lineation
	LT35 Bioclastic Pkst	3	X		X			X				Lithoclasts			Stress lineaton

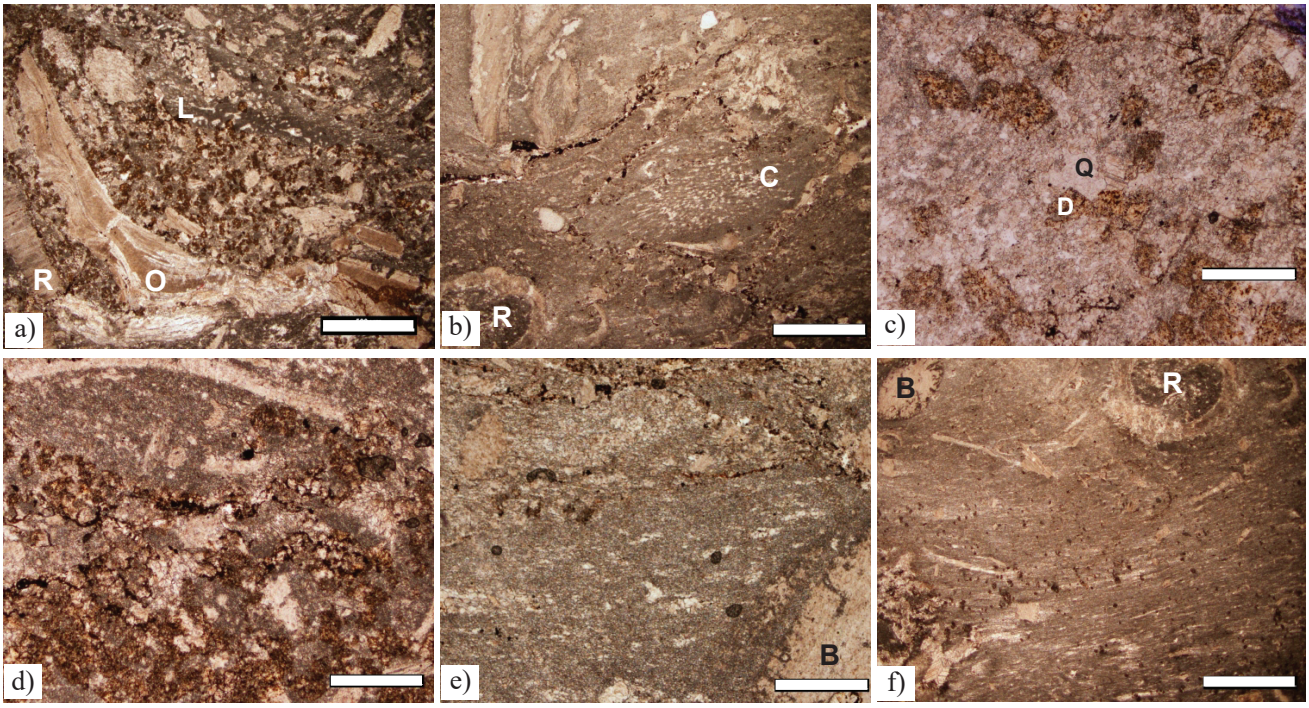

Figure 5. a) Dolomitic bivalve bioclast packstone, LT- 1; (O – oyster clast, R – rudist clast, L – *Lithocodium* encrusting bioclastic fill of oyster). b) Wackestone matrix with *Cayeuxia* nodule (C) and possible monopleurid rudist (R), LT- 2.2. c) Microspar matix with dolomite (D) growing into quartz (Q), LT- 1. d) Wavy-irregular stylolite partly filled with opaque material and dolomite, LT- 1. e) Wavy-irregular stylolites partly filled with opaque material and dolomite; bored bioclast with micrite rim (B), LT- 2. f) Lineated calcite blades and shells; in upper left-hand corner bored bioclast with micrite rim (B), to right is small oval bivalve shell, possibly a monopleurid rudist (R), LT- 2. Scale bar = 500 µm.

Table 4. Carbon and oxygen isotope values for whole rock limestones of the Los Torotes section of the Alisitos Formation.

Member/ Sample No.	$\delta^{13}C$ (‰ VPDB)	$\delta^{18}O$ (‰ VPDB)
Member E		
LT1	4.57	-8.20
LT2	4.80	-10.17
LT3	4.13	-13.37
LT5	4.34	-9.26
LT7	4.16	-10.40
LT9	4.88	-10.16
LT10	4.59	-11.06
LT14	4.45	-14.17
LT15	4.49	-9.73
Member C		
LT24	3.97	-12.61
LT25	3.68	-9.09
LT26	4.48	-8.58
LT27	4.45	-9.64
LT28	4.16	-12.99
LT31	4.39	-11.00
LT32	4.58	-10.35
LT33	3.66	-11.21
LT34	3.33	-6.84
LT35	5.26	-7.21

no echinoderm bioclasts. The upper samples have echinoderms and calcareous algae as well as bivalves. Rare are *Cayeuxia* sp. nodules (Figure 5b) and few bioclasts are bored and encrusted by micritic rims and *Lithocodium* (Figure 5a). Prismatic bivalve clasts appear to be requienid shell and small circular fossils with thick prismatic wall may be monopleurids (Figures 5a, 5b). Opaque minerals appear to be the only accessory minerals.

The micritic matrix is partly crystallized to microspar (Figure 5c. Chert partly replaces shells and in a few places matrix (Figure 5c). Wavy to irregular thin stylolites crosscut the depositional fabric (Figures 5b, 5d, 5e). Opaque grains partly replace bioclasts and matrix and line wavy stylolites (Figures 5b, 5d, 5e). The opaque material is a dull grayish-yellow color suggestive of leucoxene, and higher in the section it has the silvery color of hematite and in the upper samples pyrite is present. Stress lineations are thin elongate subparallel calcite stringers (Figures 5e, 5f) that parallel stylolites. In the upper three samples, dolomite euhedra are scattered across the matrix and replace bioclasts and intrude chert crystals, lineations and stylolites (Figures 5c, 5d). The dolomite has a golden color suggesting that it may be iron-rich, and in places dolomite includes opaque red-brown hematitic material. The resolvable paragenetic succession is: 1) encrustation of bioclasts by cyanobacteria resulting in micritic films and borings; 2) formation of opaque iron-bearing minerals; 3) recrystallization of micrite matrix; 4) chert partly replacing shells and locally matrix; 5) burial and formation of stylolites and calcite stress lineations; and 6) crystallization of fe-rich dolomite euhedra; and 7) alteration of iron-bearing minerals.

Stable isotopes

The carbon and oxygen isotopic variations are given in Table 4**.** The MC shows negative $\delta^{18}O$ values from -12.99 to -6.84‰. Likewise, the ME also shows significant negative oxygen isotope values (-14.17 to -8.2‰). Both MC and ME show positive $\delta^{13}C$ values (+3.33 to +5.26‰; +4.13 to +4.88‰; respectively).

Elemental variations

The concentrations of major oxides in limestones are given in Table 5. Both MC and ME show large variations in Al_2O_3 concentration (0.61 to 2.63%; 0.16 to 1.50%; repectively). SiO_2 concentration is higher in MC (3.40 – 28.97%) than ME (2.45 – 8.53%). The CaO concentration of limestones in ME (48.96 to 53.90%) are greater than in MC (36.99 to 52.69%). Na_2O and K_2O contents are lower in ME (0.07 to 0.48%; 0.01 to 0.40%; respectively) than in MC (0.15 to 1.21%; 0.14 to 0.93%; respectively).

The limestones of both MC and ME show large variations in Zr content (4 to 30 ppm; 3 to 20 ppm). Low contents of Co, Rb, Pb, Nb, Hf,

Table 5. Major oxides (wt%) concentrations of limestones of the Los Torotes section of the Alisitos Formation.

Member/ Sample No.	SiO_2	Al_2O_3	Fe_2O_3	CaO	MgO	K_2O	Na_2O	MnO	TiO_2	P_2O_5	LOI	Total
Member E												
LT1	2.45	0.16	0.46	53.90	0.55	0.07	0.10	0.097	0.02	0.023	42.16	99.99
LT2	4.70	0.35	0.33	52.36	0.50	0.17	0.11	0.077	0.03	0.015	41.22	99.86
LT3	3.89	0.21	0.32	52.51	0.72	0.10	0.07	0.087	0.02	0.019	42.01	99.96
LT5	3.95	0.55	0.32	52.90	0.52	0.13	0.07	0.108	0.03	0.022	41.27	99.87
LT7	3.50	0.46	0.94	51.15	2.00	0.01	0.11	0.191	0.04	0.021	41.25	99.87
LT9	8.53	1.14	0.75	48.96	0.70	0.17	0.48	0.118	0.08	0.031	38.49	99.72
LT10	5.68	1.50	0.66	51.03	0.44	0.25	0.30	0.160	0.06	0.025	39.73	99.84
LT14	4.34	1.06	0.64	52.23	0.50	0.40	0.10	0.142	0.06	0.029	40.22	99.72
LT15	3.96	0.66	0.44	51.97	0.61	0.18	0.08	0.174	0.04	0.029	41.54	99.68
Member C												
LT24	14.49	0.85	0.31	46.70	0.24	0.16	0.21	0.239	0.06	0.029	36.66	99.95
LT25	5.74	0.61	0.42	51.50	0.28	0.24	0.15	0.155	0.05	0.038	40.65	99.83
LT26	4.25	0.73	0.56	52.21	0.28	0.25	0.17	0.134	0.05	0.331	41.05	99.72
LT27	3.40	0.79	0.30	52.69	0.35	0.21	0.30	0.127	0.05	0.046	41.58	99.84
LT28	22.47	1.78	0.45	41.51	0.15	0.93	0.40	0.176	0.10	0.039	32.00	100.00
LT31	28.97	2.63	0.75	36.99	0.42	0.14	1.21	0.137	0.17	0.060	28.42	99.90
LT32	10.21	1.80	0.83	47.84	0.53	0.28	0.73	0.145	0.12	0.052	37.27	99.81
LT33	21.47	1.83	0.71	41.58	0.45	0.19	0.73	0.145	0.13	0.065	32.48	99.78
LT34	5.18	1.36	0.40	51.33	0.26	0.63	0.30	0.087	0.11	0.042	40.22	99.92
LT35	8.38	0.92	0.50	49.74	0.43	0.49	0.26	0.077	0.08	0.042	39.00	99.92

LOI: Loss on ignition.

Table 6. Trace elements (ppm) concentrations of limestones of the Los Torotes section of the Alisitos Formation.

Member/Sample No.	Co	Ni	Cr	V	Sr	Rb	Ba	Pb	Zr	Y	Nb	Hf	Th	U
Member E														
LT1	1.81	13	13	13	240	1.19	7	1.92	3	2	0.10	0.11	0.05	0.38
LT2	1.97	14	20	20	272	2.41	8	2.01	9	4	0.14	0.25	0.10	1.41
LT3	1.64	12	14	10	435	1.60	2	1.13	5	3	0.14	0.15	0.08	0.57
LT5	1.68	13	14	14	210	2.49	4	1.13	12	6	0.20	0.29	0.14	1.11
LT7	2.57	13	16	10	205	0.13	2	0.87	9	10	0.14	0.25	0.16	0.21
LT9	3.35	17	26	21	367	1.11	17	1.29	20	10	0.34	0.51	0.32	0.76
LT10	2.85	17	21	16	232	1.90	27	2.00	19	7	0.35	0.46	0.29	0.76
LT14	2.90	17	20	18	311	4.74	17	1.92	15	6	0.36	0.38	0.32	0.87
LT15	2.07	16	10	11	238	2.66	8	0.32	6	4	0.22	0.18	0.17	0.24
Member C														
LT24	2.58	17	18	17	189	3.77	28	1.95	7	10	0.36	0.23	0.21	0.83
LT25	2.44	18	14	12	237	3.00	36	1.54	12	6	0.47	0.33	0.22	0.38
LT26	2.53	19	19	12	230	3.07	54	2.99	12	5	1.29	0.34	0.29	0.55
LT27	2.90	22	19	10	269	3.14	64	2.21	4	6	0.31	0.11	0.17	0.23
LT28	3.01	15	18	12	124	15.1	222	1.47	12	15	0.61	0.31	0.64	1.74
LT31	2.71	17	12	34	222	2.68	27	1.63	30	14	0.57	0.79	0.46	1.57
LT32	2.94	19	17	19	265	4.54	58	1.78	20	8	0.49	0.53	0.19	0.38
LT33	3.11	17	11	27	157	2.38	33	0.34	18	17	0.58	0.49	0.16	0.31
LT34	4.05	26	20	39	173	3.62	102	1.78	13	5	0.26	0.36	0.17	0.92
LT35	2.83	18	8	17	354	3.24	39	0.41	13	6	0.31	0.39	0.17	0.83

Th and U are observed in the studied limestones (Table 6). Maximum concentration of Ba is found in MC (LT28: 222 ppm, Table 6). PAAS normalized trace element concentrations are plotted in Figure 6. The large-ion lithophile elements like Rb and Ba are extremely depleted compared to PAAS. The limestones are slightly enriched in Sr when compared to PAAS. The high-field strength elements (Zr, Y, Nb, Hf and Th) and ferromagnesian trace elements (Co, Ni, Cr and V) are depleted in all limestone samples with respect to PAAS.

ΣREE contents are lower in ME (2.86 – 18.96 ppm) than in MC (8.50 – 62.12 ppm; Table 7). PAAS-normalized REE patterns of the Alisitos limestones are given in Figure 7. The limestones of ME exhibit seawater-like REE+Y patterns with 1) LREE depletion (Nd_N/Yb_N = 0.32 - 0.56, 0.44 ± 0.07, n=9; Table 8; Nd_N/Yb_N of modern shallow water = 0.21 to 0.49 at 50 m water depth, Zhang and Nozaki, 1996; de Baar *et al.*, 1985; respectively), 2) negative Ce anomalies (Ce/Ce* : 0.67 - 0.94, 0.84 ± 0.09, n=9; Table 8), and 3) higher Y/Ho ratio (36.3 – 52.2, 44.0 ± 5.9, n=9; Y/Ho of seawater = 44 – 74, Bau, 1996). The limestones of MC show non-seawater-like REE+Y patterns and are significantly enriched in MREE, with lower Y/Ho ratio (33.8 – 47.4, 38.2 ± 3.8, n=10; Table 8), and less negative to positive Ce anomalies (0.84 – 1.04, 0.95 ± 0.07, n=10). ME shows greater variations in the Eu anomaly (0.79 – 2.91, 1.18 ± 0.65, n=9) than MC (0.58 – 1.13, 0.93 ± 0.19, n=10; Table 8). One sample from ME has a significantly positive Eu anomaly (Eu/Eu*: 2.91).

DISCUSSION

Depositional environments

Member C overlies a nearly 20 m-thick gypsum interval. The lower rudist packstone samples suggest a normal marine environment with rudist accumulations nearby that were established after hypersaline conditions. The overlying lime mudstone suggests that shallow shelf conditions were followed by restricted conditions such as either a deeper outer shelf or a very shallow paralic environment. The absence of microfossils in the mudstone samples suggests inhospitable conditions or unrepresentative samples. The upper interval of MC represents a return to a shallow marine shelf with rudist build-ups. The uppermost sample with chondrodonts represents a shallow marine lagoon.

In Member E, the lower interval has low diversity bivalves suggesting that salinity became less than normal. Oysters, chondrodonts(?),

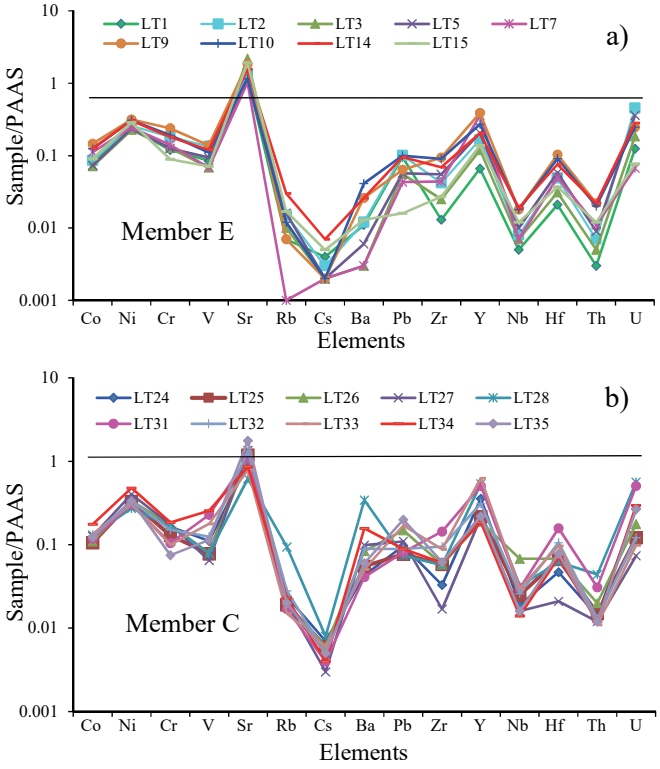

Figure 6. a) PAAS-normalized trace element diagrams for limestones of the Member C of the Alisitos Formation, and b) PAAS-normalized trace element diagrams for limestones of the Member E of the Alisitos Formation.

Table 7. Rare earth elements (ppm) concentrations of limestones of the Los Torotes section of the Alisitos Formation.

Member/Sample No.	La	Ce	Pr	Nd	Sm	Eu	Gd	Tb	Dy	Ho	Er	Tm	Yb	Lu	ΣREE
Member E															
LT1	0.77	0.66	0.12	0.54	0.14	0.04	0.17	0.02	0.15	0.03	0.10	0.01	0.09	0.01	2.86
LT2	1.65	0.99	0.33	1.49	0.39	0.09	0.49	0.07	0.43	0.09	0.28	0.04	0.26	0.04	7.62
LT3	1.42	0.63	0.27	1.18	0.28	0.07	0.36	0.05	0.28	0.06	0.19	0.03	0.18	0.02	6.03
LT5	1.86	2.56	0.42	1.90	0.52	0.12	0.63	0.10	0.60	0.13	0.39	0.05	0.37	0.05	9.69
LT7	2.50	2.82	0.51	2.33	0.65	0.46	0.86	0.14	0.85	0.20	0.61	0.08	0.60	0.08	12.68
LT9	3.07	5.20	0.80	3.76	1.07	0.20	1.30	0.20	1.23	0.27	0.81	0.11	0.83	0.12	18.96
LT10	2.90	4.48	0.64	2.92	0.76	0.18	0.94	0.14	0.81	0.17	0.51	0.07	0.49	0.07	15.10
LT14	1.93	3.12	0.48	2.19	0.58	0.13	0.72	0.11	0.67	0.15	0.44	0.06	0.45	0.06	11.09
LT15	1.31	2.26	0.35	1.59	0.44	0.10	0.53	0.08	0.47	0.10	0.30	0.04	0.30	0.04	7.91
Member C															
LT24	5.36	7.13	0.95	4.13	0.98	0.27	1.26	0.16	0.92	0.20	0.57	0.08	0.51	0.07	22.61
LT25	2.37	3.28	0.52	2.35	0.59	0.15	0.75	0.11	0.64	0.14	0.43	0.06	0.42	0.06	11.88
LT26	2.02	3.41	0.52	2.35	0.61	0.16	0.72	0.10	0.60	0.13	0.39	0.05	0.38	0.05	11.49
LT27	1.81	3.34	0.50	2.33	0.65	0.12	0.79	0.12	0.69	0.15	0.43	0.06	0.43	0.06	11.18
LT28	11.53	22.98	2.88	12.56	3.03	0.39	3.38	0.39	1.96	0.39	1.13	0.16	1.16	0.17	62.12
LT31	4.40	6.64	1.00	4.81	1.39	0.26	1.81	0.28	1.69	0.37	1.12	0.16	1.16	0.17	25.26
LT32	2.41	3.95	0.62	3.03	0.90	0.23	1.16	0.17	1.08	0.24	0.70	0.10	0.70	0.10	15.37
LT33	4.51	10.90	1.51	7.10	2.04	0.42	2.46	0.36	2.07	0.45	1.32	0.18	1.34	0.19	34.87
LT34	1.27	2.01	0.34	1.67	0.52	0.10	0.68	0.10	0.66	0.15	0.43	0.06	0.44	0.06	8.50
LT35	1.49	2.72	0.43	2.01	0.63	0.17	0.80	0.12	0.79	0.18	0.52	0.07	0.53	0.08	10.54

rudists, calcareous algae, and echinoderm clasts in the upper interval suggest that marine waters probably were near normal salinity; strong currents broke and imbricated shells probably by periodic storms. The overall depositional environment was a shallow shelf during transgression and rising sealevel.

Carbon and oxygen isotopic variations

The limestones from the entire section show distinct negative oxygen isotope values (-14.17 to -6.84‰ VPDB; Table 4; Figure 8). The most negative values are in the upper part of MC and lower part of ME. The variations in $\delta^{18}O$ compositions may be due to fluctuations in local marine baseline compositions, possibly related to climate. More negative $\delta^{18}O$ values are related to salinity and temperatures (Hudson, 1977), which suggests that cementation took place under mainly burial and/or meteoric conditions. During diagenesis, the original calcite may have been altered by calcite precipitated in the diagenetic environment, whether during burial or on the sea floor (Fisher *et al.*, 2005). Oxygen isotopic composition is more vulnerable to diagenesis than carbon isotopes, which is partly due to the temperature-related fractionation seen in oxygen isotopes (Morse and Mackenzie, 1990). The observed significant negative oxygen isotopic values in the Los Torotes section may be related to diagenetic modification. Diagenesis is also indicated by petrographic observations, which shows recrystallization of original shell minerals and stress lineations.

Modern marine carbonate sediments normally have positive ^{13}C values ranging from 0‰ to 4‰ (Hudson, 1977; Moore, 2001). Short-term variations in the $\delta^{13}C$ signals of shallow water carbonates are widely used to identify the primary variations in the Early Cretaceous oceanic $\delta^{13}C$ signature (Jenkyns, 1995; Vahrenkamp, 1996; Grötsch *et al.*, 1998). Limestones from the Los Torotes section have positive carbon isotope values (+3.33 to +5.26‰ VPDB).

Carbon isotopes are less affected by diagenesis than oxygen isotopes (Hudson, 1977; Banner and Hanson, 1990; Marshall, 1992; Frank *et al.*, 1999), because of the buffering effect of carbonate carbon in the diagenetic system (Price *et al.*, 2008). The positive correlation between carbon and oxygen values indicates diagenetic alteration of carbonate rocks (Hudson, 1977; Allen and Matthews, 1982; Fisher *et al.*, 2005). Such a positive correlation between $\delta^{13}C$ and $\delta^{18}O$ values (MC: r=0.12, n=10; ME: r=0.33, n=9; the linear correlation coefficient (r) between these isotopes is not statistically significant, see Verma, 2005, for statistical significance of r values) is lacking in the limestones

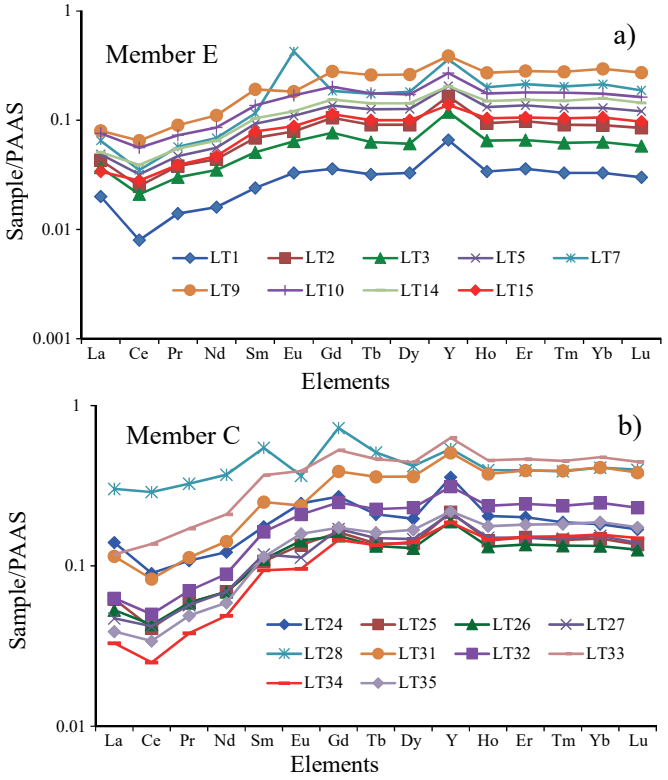

Figure 7. a) REE patterns of limestones of the Member C of the Alisitos Formation, and b) PAAS normalised REE patterns of the Member E of the Alisitos Formation.

Table 8. Elemental ratios of limestones of the Los Torotes section of the Alisitos Formation.

Member/Sample No.	La/Sc	La/Co	Nd_N/Yb_N	La_N/Yb_N	Y/Ho	Ce/Ce*	Eu/Eu*	ΣREE
Member E								
LT1	1.88	0.42	0.48	0.61	52.2	0.67	1.12	3.12
LT2	2.13	0.83	0.49	0.48	47.9	0.78	0.93	8.32
LT3	1.87	0.87	0.56	0.59	50.1	0.84	1.02	6.51
LT5	2.12	1.11	0.43	0.38	42.6	0.84	0.98	10.7
LT7	2.12	0.97	0.32	0.31	49.0	0.78	2.91	14.3
LT9	0.95	0.92	0.38	0.27	39.0	0.94	0.79	21.1
LT10	1.43	1.02	0.49	0.43	41.8	0.93	1.02	16.4
LT14	1.09	0.67	0.41	0.32	37.3	0.87	0.95	12.3
LT15	1.35	0.63	0.44	0.32	36.3	0.90	0.93	8.7
Member C								
LT24	3.65	2.08	0.67	0.77	47.4	0.96	1.13	24.0
LT25	2.06	0.97	0.47	0.42	41.0	0.84	1.03	13.0
LT26	1.60	0.80	0.52	0.40	39.0	0.88	1.11	12.5
LT27	1.13	0.62	0.45	0.31	38.5	0.93	0.80	12.6
LT28	4.87	3.83	0.90	0.74	37.0	1.03	0.58	65.1
LT31	0.93	1.62	0.34	0.28	37.0	0.99	0.76	28.2
LT32	0.80	0.82	0.36	0.26	35.8	0.98	1.04	17.2
LT33	1.37	1.45	0.44	0.25	37.7	1.04	0.89	38.4
LT34	0.41	0.31	0.31	0.21	34.8	0.93	0.82	9.7
LT35	0.71	0.53	0.31	0.21	33.8	0.87	1.13	11.9

from MC and ME of Los Torotes section (Figure 8). This suggests that the carbon isotopic values unchanged during diagenesis (*e.g.*, Jenkyns, 1974; 1996; Jenkyns and Clayton, 1986).

Behaviour of Europium

Limestones of ME and MC have both negative and positive Eu anomalies (Eu/Eu*: 0.79 – 2.91; 0.58 – 1.13; respectively, Table 8). REE composition of modern clastic sediments and seawater chemical precipitates mainly display the composition of the upper crustal rocks, which have distinctly negative Eu anomalies (Piper, 1974; Elderfield and Greaves, 1982). PASS-normalized positive Eu anomalies are not common in seawater. Positive values result from hydrothermal solutions (Michard *et al.*, 1983; Klinkhammer *et al.*, 1983,; German *et al.*, 1993; Sherrell *et al.*, 1999), from sediments affected by diagenesis (MacRae *et al.*, 1992), by enrichment of feldspar (Murray *et al.*, 1991; Madhavaraju and Ramasamy, 1999; Madhavaraju and Lee, 2009; Madhavaraju *et al.*, 2010, 2016), by sediments derived from high T-basalt alteration along mid-ocean ridges, or from back arc spreading centres (Michard *et al.*, 1983; German *et al.*, 1993; Siby *et al.*, 2008).

MacRae *et al.* (1992) noted that Amazon fan muds exhibit significant positive Eu anomalies, because of precipitation of Eu^{2+} from pore waters during diagenesis. Eu content is positively correlated with Y in limestones from both MC and ME (r=0.95, 0.80, respectively; Figure 9a) and reveals the non-diagenetic origin of this element. The inclusion of small amounts of detrital feldspars may lead to positive Eu anomalies in the bulk sediments (Murray *et al.*, 1991; Madhavaraju and Lee, 2009; Madhavaraju *et al.*, 2010). In addition, Al_2O_3 is not correlated with Eu/Eu* (MC: -0.57; ME: -0.25; respectively; Figure 9b). Hence the positive Eu anomalies in these limestones seem to have not been influenced by the amount of feldspars in them. Because intense diagenesis or higher feldspar content are not reported from these limestones, the positive Eu anomalies observed here may be due to hydrothermal fluids or co-precipitation of hydrothermal Fe-sulphides.

The Eu^{3+}/Eu^{2+} redox potential in aqueous solutions mainly depends on variations in temperatures and to a minor extent on pressure, pH and REE speciation (Bau, 1991), which explains the positive Eu anomalies found in acidic, reducing hydrothermal fluids (Kamber *et al.*, 2004). Eu/Eu* ratios of the Alisitos limestones exhibit no correlation with Pr_N/Yb_N (MC: -0.22; ME: -0.54; respectively; Figure 9c) and Pr_N/Sm_N (MC: 0.14; ME: -0.22; respectively; Figure 9d) ratios. This implies that Eu was decoupled from other redox-sensitive REEs due to the interaction of hydrothermal solutions with Cretaceous seawater during the deposition of limestones of the Alisitos Formation. The Rosario segment of the Alisitos arc was the site of several hydrothermal activities during the Early Cretaceous (Busby *et al.*, 2006). In the northern part of the Nuevo Rosarito plutonic suite, diorite of Lower Cretaceous age is cut by numerous amphibole veins of probable hydrothermal origin (Peña-Alonso *et al.*, 2012). In addition, Peña-Alonso *et al.* (2012) identified altered pyroxene (moderately altered to uralite) in Lower Cretaceous gabbroic rock which produced by scavenging hydrothermal activity. These observations suggest that the sedimentary basin might have been affected by hydrothermal events during Early Cretaceous. Thus, the observed positive Eu anomalies in many samples may be the product of hydrothermal fluids or co-precipitation of hydrothermal Fe-sulfide.

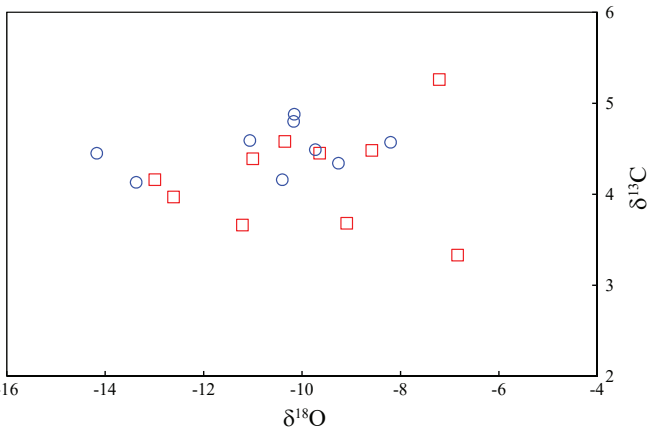

Figure 8. $\delta^{13}C$ versus $\delta^{18}O$ bivariate plot for limestones of the Alisitos Formation (Symbols: □ - Member E; ○ - Member C).

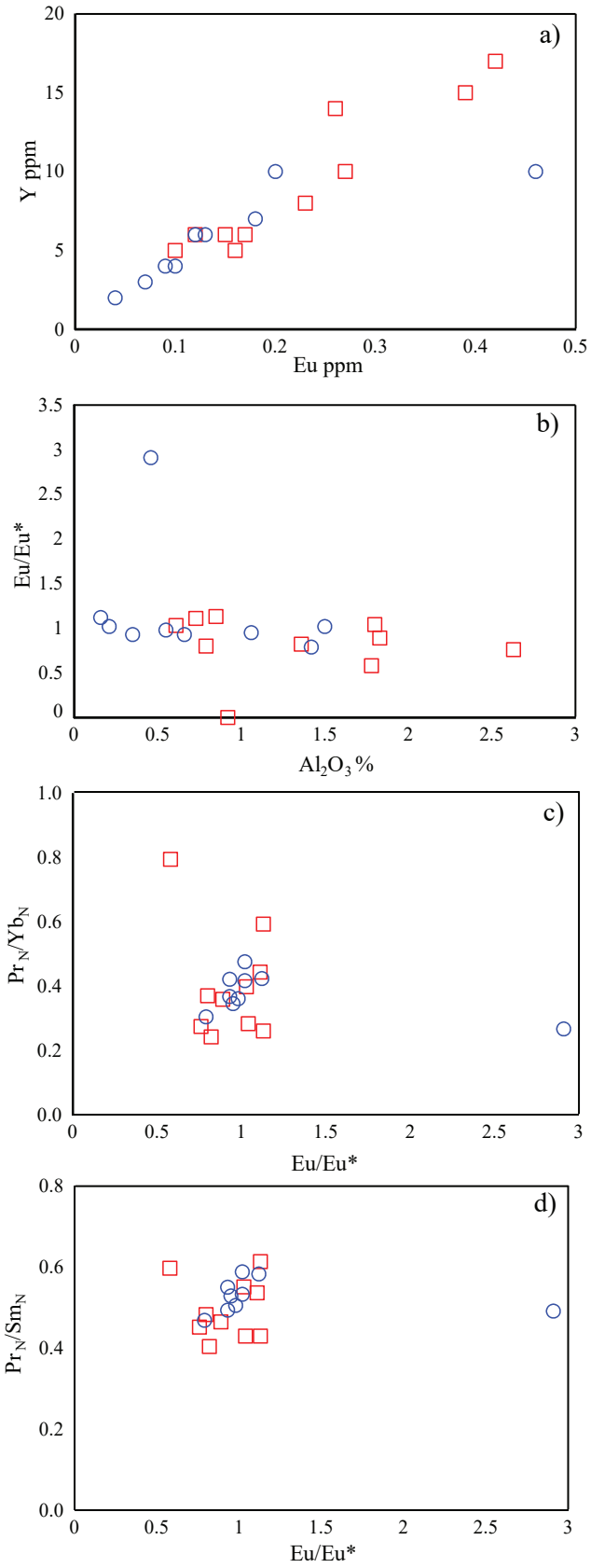

Figure 9. a) Y vs Eu bivariate plot, b) Eu/Eu* *vs*. Al_2O_3 bivariate plot, c) Pr_N/Yb_N *vs*. Eu/Eu* bivariate plot and d) Pr_N/Sm_N *vs*. Eu/Eu* bivariate plot for limestones of the Alisitos Formation (Symbols: □ - Member E; ○ - Member C).

Possible source of REEs in the Alisitos Formation

The evaluation of seawater chemistry in the geological past is mainly dependent upon geochemical proxies thought to reflect contemporaneous seawater composition. Recent studies have shown that microbial carbonates are considered to be reliable proxies for assessment of ancient seawater REE geochemical signatures (Webb and Kamber, 2000; Olivier and Boyet, 2006; Oliveri *et al.*, 2010).

The ΣREE content of limestoens of the Alisitos Formation is moderately positively correlated with elements representative of fine-grained and sand-sized detritus such as Al and Si (r=0.64; r=0.80; respectively). However, the correlation between Nd_N/Yb_N and Al_2O_3 of the samples is negative (r= -0.29, n=19). Hence, the absence of a positive correlation between Nd_N/Yb_N and Al_2O_3 may result from sample heterogeneity. In any case, a high Al_2O_3 content is not correlated with and low LREE depletion (high Nd_N/Yb_N) in the studied limestones. The La_N/Yb_N ratios of the limestones (MC: 0.21 – 0.77; ME: 0.27 – 0.61; Table 8) are significantly lower than the values proposed by Condie (1991; about 1.0) and Sholkovitz (1990; about 1.3) for terrigenous materials. In addition, the relative REE contents in the limestones can be tested using the parameters, such as Pr_N/Sm_N and Pr_N/Nd_N, which do not correlate with Al_2O_3 and ΣREE contents.

The limestones of Member C have non-seawater-like REE+Y patterns whereas limestones of Member E show distinctly seawater-like patterns (Figure 7). The non-seawater-like patterns result from the presence of detrital contaminants that effectively mask a seawater signature in the limestone because of their high REE concentrations (flat pattern: German and Elderfield, 1990; Elderfield *et al.*, 1990; Bau and Dulski, 1996; Webb and Kamber, 2000). The inclusion of terrigenous materials in the limestones may be assessed by determining the abundance of Al_2O_3 and Th (Nothdurft *et al.*, 2004). The concentration of Al_2O_3 is lower in Member E (0.71 ± 0.5, n=9) than in Member C (1.33 ± 0.66, n=10) (Table 5). Fe_2O_3 content of Member E correlates well with the abundances of Zn, Mn, Co, Eu, Y and ΣREE whereas the limestones of Member C show no such correlation with these elements. These elements are known to be partially associated with or incorporated into amorphous Fe and Mn oxyhydroxides which suggests hydrothermal events affected Member E of the Alisitos Formation. Hydrothermal input is a source of Fe and Mn oxyhydroxides, which incorporates REEs disproportionately and unpredictably. However, this input was not strong enough to obscure the REE geochemistry of seawater in the limestones of Member E during the Albian.

The limestones of Member E have distinct seawater-like REE+Y patterns (Figure 10a), which compare with modern seawaters (Figure 10b) and marine limestones yielding similar REE patterns (Figure 10c; Upper Devonian carbonate sediments, Nothdurft *et al.*, 2004; Permian Limestone, Kawabe *et al.*, 1991; Mural Limestone, Madhavaraju and González-León, 2012; Albian-Cenomanian Limestone, Bellanca *et al.*, 1997; Holocene reefal microbialite, Webb and Kamber, 2000). However, Member C exhibits non-seawater-like patterns, which compare with other limestones that exhibit non-seawater-like patterns (Figure 11; Upper Devonian coastal fringing reef, Nothdurft *et al.*, 2004; Aptian-Albian limestone: Madhavaraju *et al.*, 2010; Albian limestone, Madhavaraju and Lee, 2009; Maastrichtian limestone, Madhavaraju and Ramasamy, 1999; Miocene limestone, Armstrong-Altrin *et al.*, 2003). This suggests that the inclusion of terrigenous materials in carbonates as contaminants will mask the seawater signature because of their high REE concentration.

The concentrations of certain immobile elements like La and Th are higher in silicic than in basic igneous rocks and aid in identifying the source rocks of terrigenous materials (Cullers, 1995). The felsic and mafic rocks show significant variations in La/Sc, La/Co, Th/Sc, Th/Co and Th/Cr ratios which are most useful in understanding the

provenance composition (Wronkiewicz and Condie, 1990; Cox *et al.*, 1995; Cullers, 1995). The extent to which these elemental ratios are useful in unraveling the provenance of terrigenous materials present in the carbonate rock is clearly addressed by Cullers (2002). The La/Sc, La/Co and Eu/Eu* ratios of the Los Torotes MC limestones are comparable to fine fractions of felsic and mafic rocks, and with upper continental crust (UCC) and PAAS values (Table 9). It suggests that terrigenous materials present in MC were derived from mafic to felsic source rocks. Furthermore, our results are consistent with the Cretaceous geology of Baja California (Suárez-Vidal, 1987; Busby, 2004).

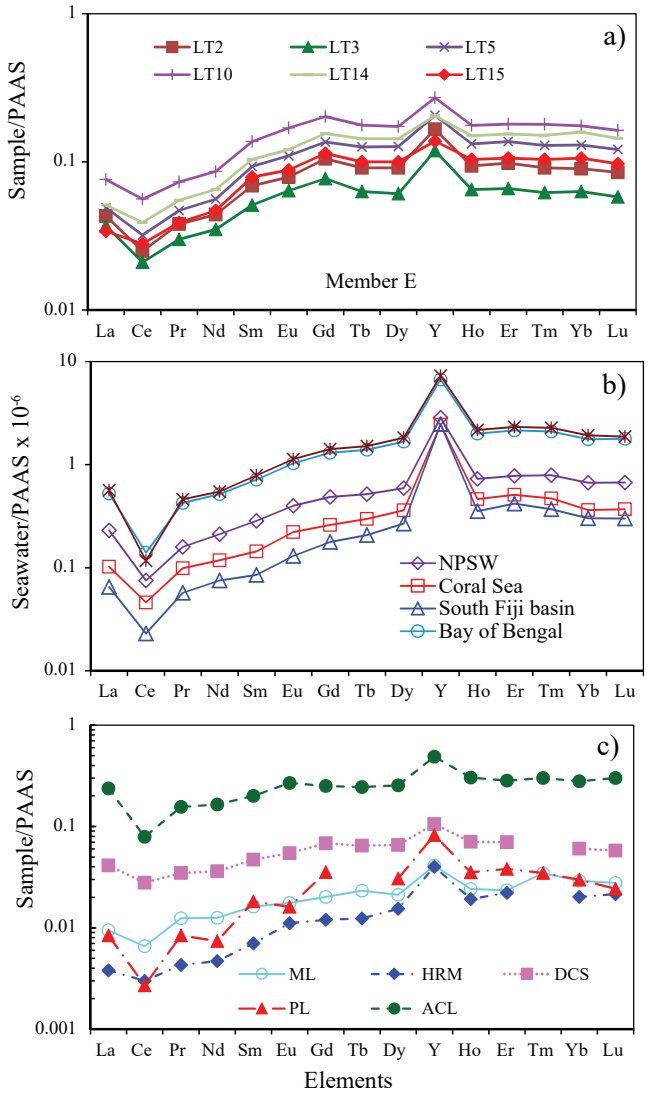

Figure 10. a) PAAS normalized REE patterns of representative samples of the Member E compared with, b) PAAS normalized REE patterns of modern seawaters (NPSW: North Pacific shallow water, Sagami trough (Alibio and Nozaki, 1999), Coral Sea: Coral sea (South Pacific shallow seawater, Zhang and Nozaki, 1996), South Fiji Basin: South Fiji Basin - Station SA12 (Zhang and Nozaki, 1996), Bay of Bengal: Bay of Bengal shallow water (Nozaki and Alibio, 2003) and Andaman Sea: Andaman Sea shallow water (Nozaki and Alibio, 2003), and c) PAAS normalized REE patterns of marine limestones yielding similar REE patterns (Upper Devonian carbonate sediments, Nothdurft *et al.*, 2004; Permian Limestone, Kawabe *et al.*, 1991; Mural Limestone, Madhavaraju and Gonzalez-Leon, 2012; Albian-Cenomanian Limestone, Bellanca *et al.*, 1997; Holocene reefal microbialite, Webb and Kamber, 2000).

CONCLUSIONS

Limestones of the Alisitos Formation collected from the Los Torotes section are mudstone, wackstone and packstone lithofacies. The presence of corals and rudist bivalves in a fine-grained matrix in the lower part of the section indicates normally quiet and relatively shallow marine conditions of a lagoon or inner shelf setting. In addition, the upper part of the section has caprinid, rudists and calcareous green algae (*Cayeuxia*) assemblages, which also supports shallow marine depositional environment for the Alisitos Formation. The limestones have large variations in both $\delta^{13}C$ and $\delta^{18}O$ values. The lack of positive correlation between $\delta^{13}C$ and $\delta^{18}O$ values indicates that the $\delta^{13}C$ values measured in the Los Torotes section are primary in nature.

The limestones of ME exhibit seawater-like REE+Y patterns whereas MC has non-seawater-like REE+Y patterns. Fe_2O_3 content of ME correlates well with the abundances of Zn, Mn and Co and Eu, Y and ΣREE whereas MC reveals no such correlation with these elements. These elements are known to be partially associated or incorporated into amorphous Fe and Mn oxyhydroxides which suggest hydrothermal events during deposition of ME of the Alisitos Formation. The seawater-like-REE patterns in limestones of ME suggests that most of the REEs present in them were derived from the seawater rather than detrital materials. However, MC contains significant amount of terrigenous contaminants, which effectively mask the seawater signatures owing to their elevated REE concentrations. Both MC and ME show negative and positive Eu anomalies. The observed positive Eu anomalies in many samples may be the product of hydrothermal

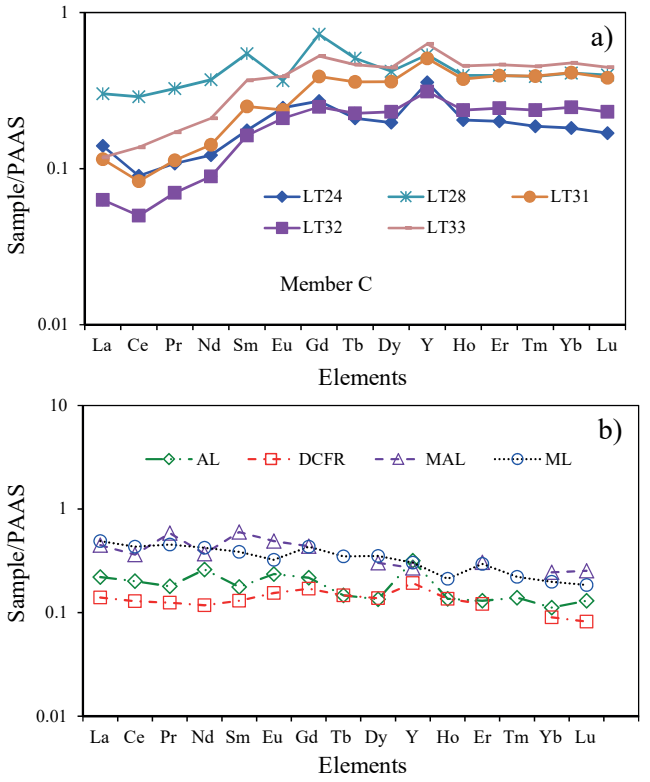

Figure 11. PAAS normalized REE patterns of the Member C are compared with limestones exhibit non-seawater-like signatures (DCFR: Late Devonian coastal fringing reef (Nothdurft *et al.*, 2004), AL: Albian limestone (Madhavaraju and Lee, 2009), MAL: Maastrichtian limestone (Madhavaraju and Ramasamy, 1999) and ML: Miocene limestone (Kudankulam Formation, Armstrong-Altrin *et al.*, 2003).

Table 9. Range of elemental ratios of Member C of Alisitos Formation compared to felsic rocks, mafic rocks, Upper Continental Crust (UCC) and Post-Archaean Australian Shale (PAAS).

Elements ratios	Alisitos Formation[a]	Range of sediments[b]		UCC[c]	PAAS[c]
	Member C	Felsic rocks	Mafic rocks		
Eu/Eu*	0.93	0.40 – 0.94	0.71 – 0.95	0.63	0.66
La/Sc	0.41 – 4.87	2.50 – 16.3	0.43 – 0.86	2.21	2.40
La/Co	0.31 – 3.83	1.04 – 13.8	0.14 – 0.38	1.76	0.90
ΣREE	23	–	–	–	185

[a] Present study n=10; [b] Cullers (1994, 2000), Cullers and Podkovyrov, 2000; [c] Taylor and McLennan, 1985.

fluids or co-precipitation of hydrothermal Fe-sulfide. The elemental ratios like La/Sc, La/Co and Eu/Eu* suggest mafic to felsic sources for the terrigenous particles present in the MC limestones,

ACKNOWLEDGEMENTS

We acknowledge the support provided by Universidad Nacional Autonoma de Mexico through PAPIIT Project No.IN110909-3. This work represents part of an MSc thesis completed by Satheesan Sandeep. We would like to thank Dr. Farah H. Tobia and an anonymous reviewers for their critical reviews and constructive comments. We thank scientific editor, Dr. Thomas Lehmann for his comments and useful suggestions. We would like to thank Mr. Pablo Peñaflor for powdering of limestone samples for geochemical and isotope studies. We thank Mrs. Adriana Aime Orci Romero for preparing thin sections for petrographic study. We also thank Mr. Rufino Lozano and Ms. R. P. Girón García, Instituto de Geología, Universidad Nacional Autonoma de México, México for their help in XRF analysis.

REFERENCES

Alibio, D.S., Nozaki, Y., 1999, Rare earth elements in seawater: Particle association, shale-normalisation, and Ce oxidation: Geochimica et Cosmochimica Acta, 63, 363-372.

Allan, J.R., Matthews, R.K., 1982, Isotope signatures associated with early meteoric diagenesis: Sedimentology, 29, 797-817.

Allison, E.C., 1955, Middle Cretaceous gastropoda of Punta China, Baja California, Mexico: Journal of Paleontology, 29, 400-432.

Allison, E.C., 1974, The type Alisitos Formation (Cretaceous, Aptian-Albian) of Baja California and its bivalve fauna, in Gastil, R.G., Lillegaven, J. (eds.), Geology of peninsular California, Pacific Section: American Association Petroleum Geologists, Society of Economic Paleontologists and Mineralogists and Society of Engineering Geologists, Guidebook, 29-59.

Almazan-Vázquez, E., 1988, Marco paleosedimentario y geodinamico de la Formación Alisitos en la Península de Baja California: Instituto de Geología Universidad Nacional Autónoma de México, Revista, 7, 41-51.

Almazán-Vázquez, E., Buitrón-Sánchez, B.E., 1984, Bioestratigrafía del Cretácico inferior de Baja California Norte, Mexico, *in* Perrilliat, M. (ed.), Universidad Nacional Autónoma de México Congreso Latinoamericano de paleontología, Mexico City, Memoria III, 378-387.

Armstrong-Altrin, J.S., Verma, S.P., Madhavaraju, J., Yong, I.L., Ramasamy, S., 2003, Geochemistry of Late Miocene Kudankulam Limestones, South India: International Geology Review, 45, 16-26.

Armstrong-Altrin, J.S., Madhavaraju, J., Sial, A.N., Kasper-Zubillaga, J.J., Nagarajan, R., Flores-Castro, K., Rodríguez, J.L., 2011, Petrography and stable isotope geochemistry of the Cretaceous El Abra Limestones (Actopan), Mexico: Implication on diagenesis: Journal of the Geological Society of India, 77, 349-359.

Banner, J.L., Hanson, G.N., 1990, Calculation of simultaneous isotopic and trace element variations during water-rock interaction with applications to carbonate diagenesis: Geochemica et Cosmochimica Acta, 54, 3123-3137.

Bau, M., 1991, Rare earth element mobility during hydrothermal and metamorphic fluid-rock interaction and the significance of the oxidation state of europium: Chemical Geology, 93, 219-230.

Bau, M., 1996, Controls on fractionation of isovalent trace elements in magmatic and aqueous systems: Evidence from Y/Ho, Zr/Hf and lanthanide tetrad effect: Contribution to Mineralogy and Petrology, 123, 323-333.

Bau, M., Dulski, P., 1996, Distribution of yttrium and rare earth elements in the Penge and Kuruman iron formation, Transvaal Supergroup, South Africa: Precambrian Research, 79, 37-55.

Beggs, J.M., 1984, Volcaniclastic rocks of Alisitos Group, Baja California, Mexico, in Frizzel V.A. Jr. (ed.), Geology of the Baja California Peninsula: Society of Economic Paleontologists and Mineralogists Pacific Section, 39, 43-52.

Bellanca, A., Masetti, D., Neri, R., 1997, Rare earth elements in limestone/marlstone couplets from the Albian-Cenomanian Cismon section (Venetian region, northern Italy): assessing REE sensitivity to environmental changes: Chemical Geology, 141, 141-152.

Bolhar, R., Van Kranendonk, M.J., 2007, A non-marine depositional setting for the northern Fortescue Group, Pilbara Craton, inferred from trace element geochemistry of stromatolitic carbonates: Precambrian Research, 155, 229-250.

Bolhar, R., Kamber, B.S., Moorbath, S., Fedo, C.M., Whitehouse, M.J., 2004, Characterisation of early Archaean chemical sediments by trace element signatures: Earth and Planetary Science Letters, 222, 43-60.

Busby, C., 2004, Continental growth at convergent margins facing large ocean basins: a case study from Mesozoic convergent-margin basins of Baja California, Mexico: Tectonophysics, 392, 241-277.

Busby, C., Adams, B.F., Mattinson, J., Deoreo, S., 2006, View of an intact oceanic arc, from surficial to mesozonal levels: Cretaceous Alisitos arc, Baja California: Journal of Volcanology and Geothermal Research, 149, 1- 46.

Campa, M.F., Coney, P.J., 1983, Tectono-stratigraphic terranes and mineral resource distributions in Mexico: Canadian Journal Earth Science, 20, 1040-1051.

Condie, K.C., 1991, Another look at rare earth elements in shales: Geochimica et Cosmochimica Acta, 55, 2527-2531.

Cox, R., Lowe, D.R., Cullers, R.L., 1995, The influence of sediment recycling and basement composition on evolution of mudrock chemistry in the southwestern United States: Geochimica et Cosmochimica Acta, 59, 2919-2940.

Craig, H., 1957, Isotopic standards for carbon and oxygen and correction factors for mass spectrometric analyses of carbon dioxide: Geochimica et Cosmochimica Acta, 12, 133-149.

Cullers, R.L., 1994, The controls on the major and trace element variation of shales, siltstones and sandstones of Pennsylvanian – Permian age from uplifted continental blocks in Colorado to platform sediment in Kansas, USA: Geochimica et Cosmochimica Acta, 58, 4955-4972.

Cullers, R.L., 1995, The controls on the major and trace element evolution of shales, siltstones and sandstones of Ordovician to Tertiary age in the Wet Mountain region, Colorado, U.S.A.: Chemical Geology, 123, 107-131.

Cullers, R.L., 2000, The Geochemistry of shales, siltstones and sandstones of Pennsylvanian-Permian age, Colorado, USA: implications for provenance and metamorphic studies: Lithos, 51, 305-327.

Cullers, R.L., 2002, Implications of elemental concentrations for provenance, redox conditions, and metamorphic studies of shales and limestones near Pueblo, CO, USA: Chemical Geology, 191, 305-327.

Cullers, R.L., Podkvyrov, V.N., 2000, Geochemistry of the Mesoproterozoic Lakhanda shales in southeastern Yakutia, Russia: Implications for mineralogical and provenance control, and recycling: Precambrian Research, 104, 77-93.

De Baar, H.J.W., Bacon, M.P., Brewer, P.G., 1985, Rare earth elements in the Pacific and Atlantic oceans: Geochemica et Cosmochimica Acta, 49, 1943-1959.

De Baar, H.J.W., Schijf, J., Byrne, R.H., 1991, Solution chemistry of the rare earth elements in seawater: European Journal of Solid State and Inorganic Chemistry, 28, 357-373.

Eggins, S.M., Woodhead, J.D., Kinsley, L.P.J., Mortimer, G.E., Sylvester, P., McCulloch, M.T., Hergt, J.M., Handler, M.R., 1997, A simple method for the precise determination of >=40 trace elements in geological samples by ICPMS using enriched isotope internal standardization: Chemical Geology, 134, 311-326.

Elderfield, H., 1988, The oceanic chemistry of the rare earth elements: Philosophical Transactions of the Royal Society of London A, 325, 105-126.

Elderfield, H., Greaves, M.J., 1982, The rare earth elements in seawater: Nature, 296, 214-219.

Elderfield, H., Upstill-Goddard, R., Sholkovitz, E.R., 1990, The rare earth elements in rivers, estuaries and coastal seas and their significance to the composition of ocean waters: Geochimica et Cosmochimica Acta, 54, 971-991.

Fisher, J.K., Price, G.D., Hart, M.B., Leng, M.J., 2005, Stable isotope analysis of the Cenomanian-Turonian (Late Cretaceous) oceanic anoxic event in the Crimea: Cretaceous Research, 26, 853-863.

Frank, T.D., Arthur, M.A., Dean, W.E., 1999, Diagenesis of Lower Cretaceous pelagic carbonates, North Atlantic: paleoceanographic signals obscured: Journal of Foraminiferal Research, 29, 340-351.

Garcia, M.G., Lecomte, K.L., Pasquini, A.I., Formica, S.M., Depetris, P.J., 2007, Sources of dissolved REE in mountain streams draining granitic rocks, sierras Pampeanas, Cordoba, Argentina: Geochimica et Cosmochimica Acta, 71, 5355-5368.

German, C.R., Elderfield, H., 1990, Application of Ce anomaly as a paleo redox indicator: the ground rules: Paleoceanography, 5, 823-833.

German, C.R., Holliday, B.P., Elderfield, H., 1993, A geochemical study of metalliferous sediment from the TAG hydrothermal mound, 26º08' N, Mid-Atlantic ridge: Journal of Geophysical Research, 98, 9683-9692.

Govindaraju, K., 1994, Compilation of Working Values and Sample Description for 383 standard reference materials: Geostandards Newsletters, 18, 331 pp.

Greaves, M.J., Elderfield, H., Sholkovitz, E.R., 1999, Aeolian sources of rare earth elements to the Western Pacific Ocean: Marine Chemistry, 68, 31-38.

Grötsch, J., Billing, I., Vahrenkamp, V., 1998, Carbon-isotope stratigraphy in shallow water carbonates: implications for Cretaceous black-shale deposition: Sedimentology, 45, 623-634.

Hudson, J.D., 1977, Stable isotopes and limestone lithification: Journal of Geological Society of London, 133, 637-660.

Jenkyns, H.C., 1974, Origin of red nodular limestones (Ammonitico Rosso Knollenkalke) in the Mediterranean Jurassic: A diagenetic model, in Pelagic Sediments on Land and Under the Sea, In Hsu, K.J., Jenkyns, H.C. (eds.), International Association of Sedimentologists: Cambridge, Special Publication Blackwell, 1, 49-271.

Jenkyns, H.C., 1995, Carbon isotope stratigraphy and paleoceanographic significance of the Lower Cretaceous shallow-water carbonates of Resolution Guyot, Mid-Pacific Mountains: Proceedings of Ocean Drilling Program, Scientific Results, 143, 99-104.

Jenkyns, H.C., 1996, Relative sea-level change and carbon isotope: Data from the Upper Jurassic (Oxfordian) of central and southern Europe: Terra Nova, 8, 75-85.

Jenkyns, H.C., Clayton, C.J., 1986, Black shales and carbon isotopes in pelagic sediments from the Tethyan Lower Jurassic: Sedimentology, 33, 87-106.

Kawabe, I., Kitahara, Y., Naito, K., 1991, Non-chondritic yttrium/holmium ratio and lanthanide tetrad effect observed in pre-Cenozoic limestones: Geochemical Journal, 25, 31-44.

Klinkhammer, G., Elderfield, H., Hudson, A., 1983, Rare earth elements in seawater near hydrothermal vents: Nature, 305, 185-188.

Lachance, G.R., Traill, R.J., 1966, A practical solution to the matrix problem in X-ray analysis, I. Method: Canadian Spectroscopy, 11, 43-48.

Liu, Y.G., Miah, M.R.U., Schmitt, R.A., 1988, Cerium: a chemical tracer for paleo-oceanic redox conditions: Geochimica et Cosmochimica Acta, 52, 1361-1371.

MacRae, N.D., Nesbitt, H.W., Kronberg, B.I., 1992, Development of a positive Eu anomaly during diagenesis: Earth and Planetary Science Letters, 109, 585-591.

Madhavaraju, J., González-León, C.M., 2012, Depositional conditions and source of rare earth elements in carbonate strata of the Aptian-Albian Mural Formation, Pitaycachi section, northeastern Sonora, Mexico: Revista Mexicana de Ciencias Geológicas, 29, 478-491.

Madhavaraju, J., Lee, Y.I., 2009, Geochemistry of the Dalmiapuram Formation of the Uttatur Group (Early Cretaceous), Cauvery Basin, southeastern India: Implications on provenance and paleo-redox conditions: Revista Mexicana de Ciencias Geológicas, 26, 380-394.

Madhavaraju, J., Ramasamy, S., 1999, Rare earth elements in limestones of Kallankurichchi Formation of Ariyalur Group, Tiruchirapalli Cretaceous, Tamil Nadu: Journal of the Geological Society of India, 54, 291-301.

Madhavaraju, J., González-León, C.M., Lee, Y.I., Armstrong-Altrin, J.S., Reyes-Campero, L.M., 2010, Geochemistry of the Mural Formation (Aptian-Albian) of the Bisbee Group, Northern Sonora, Mexico: Cretaceous Research, 31, 400-414.

Madhavaraju, J., Lee, Y.I., Gonzólez-Leon, C.M., 2013a, Carbon, oxygen and strontium isotopic signatures in Aptian-Albian limestones of the Mural Formation, Cerro Pimas area, northern Sonora, Mexico: Journal of Iberian Geology. 39, 73-88.

Madhavaraju, J., Sial, A.N., González-León, C.M., Nagarajan, R., 2013b, Carbon and oxygen isotopic variations in Early Albian limestone facies of the Mural Formation, Pitaycachi section, northeastern Sonora, Mexico: Revista Mexicana de Ciencias Geologicas, 30, 526-539.

Madhavaraju, J., Löser, H., Lee, Y.I., Lozano-SantaCruz, R., Pi-Puig, T., 2016, Geochemistry of Lower Cretaceous limestones of the Alisitos Formation, Baja California, Mexico: implications for REE source and paleo-redox conditions: Journal of South American Earth Science, 66, 149-165.

Marshall, J.D., 1992, Climatic and oceanographic isotopic signals from the carbonate rock record and their preservation: Geological Magazine, 129, 143-160.

Michard, A., Albarede, F., Michard, G., Minister, J.F., Charlow, J.L., 1983, Rare earth elements and uranium in high temperature solutions from East-Pacific rise hydrothermal vent field (13ºN): Nature, 303, 795-797.

Moore, C.H., 2001, Carbonate Reservoirs: Porosity evolution and diagenesis in a sequence stratigraphic framework: Amsterdam, Developments in Sedimentology, Elsevier, 444 pp.

Morse, J.W., MacKenzie, F.T., 1990, Geochemistry of sedimentary carbonates: Developments in Sedimentology 48, 707 pp.

Morán-Zenteno, D., 1994, The Geology of the Mexican Republic. AAPG Studies in Geology. Tulsa, OK, USA: American Association of Petroleum Geologist, 167 pp.

Moullade, M., Kuhnt, W., Bergen, J.A., Masse, J.P., Tronchetti, G., 1998, Correlation of biostratigraphic and stable isotope events in the Aptian historical stratotype of La Bédoule (southeast France): Comptes Rendus de l'Académie des Sciences, Paris Série IIA Sciences de la Terre et des Planètes, 327, 693-698.

Murray, R.W., Ten Brink, M.R.B., Brumsack, H.J., Gerlach, D.C., Russ III, G.P., 1991, Rare earth elements in Japan Sea sediments and diagenetic behaviour of Ce/Ce*: Results from ODP Leg 127: Geochimica et Cosmochimica Acta, 55, 2453-2466.

Nagarajan, R., Madhavaraju, J., Armstron-Altrin, J.S., Nagendra, R., 2011, Geochemistry of Neoproterozoic limestones of the Shahabad Formation, Bhima Basin, Karnataka, southern India: Geoscience Journal, 15, 9-25.

Nothdurft, L.D., Webb, G.E., Kamber, B.S., 2004, Rare earth element geochemistry of Late Devonian reefal carbonates, Canning Basin, Western Australia: Confirmation of a seawater REE proxy in ancient limestone: Geochimica et Cosmochimica Acta, 68, 263-283.

Nozaki, Y., Alibio, D.S., 2003, Importance of vertical geochemical processes in controlling the oceanic profiles of dissolved rare earth elements in northeastern Indian Ocean: Earth and Planetary Science Letters, 205, 155-172.

Oliveri, E., Neri, R., Bellanca, A., Riding, R., 2010, Carbonate stromatolites from a Messinian hypersaline setting in the Caltanissetta Basin, Sicily: petrographic evidence of microbial activity and related stable isotope and

rare earth element signatures: Sedimentology, 57, 142-161.
Olivier, N., Boyet, M., 2006, Rare earth and trace elements of micorbialites in Upper Jurassic coral and sponge-microbialite reef: Chemical Geology, 230, 105-123.
Peña-Alonso, T.A., Delgado-Argote, L.A., Weber, B., Velasco-Tapía, F., Valencia, V., 2012, Geology and emplacement history of the Nuevo Rosarito plutonic suite in the southern Peninsular Ranges batholith, Baja California, México: Revista Mexicana de Ciencias Geológicas, 29(1), 1-23.
Piper, D.Z., 1974, Rare earth elements in the sedimentary cycle, a summary: Chemical Geology, 14, 285-304.
Price, G.D., Dashwood, B., Taylor, G.K., Kalin, R.M., Ogle, N., 2008, Carbon isotope and magnetostratigraphy of the Cretaceous (Barremian-Aptian) Pabellon Formation, Chañarcillo Basin, Chile: Cretaceous Research, 29, 183-191.
Santillan, M., Barrera, T., 1930, Las posibilidades petrolíferas en la costa occidental de la Baja California, entre los paralelos 30 y 32 de latitud norte: Instituto de Geología, Mexico, Anales 5, 1-37.
Scholle, P.A., Arthur, M.A., 1980, Carbon isotope fluctuations in Cretaceous pelagic limestones: Potential stratigraphic and petroleum exploration tool: Bulletin American Association of Petroleum Geologists, 64, 67-87.
Sherrell, R.M., Field, M.P., Ravizza, G., 1999, Uptake and fractionation of rare earth elements on hydrothermal plume particles at 945´ N, East Pacific Rise: Geochimica et Cosmochimica Acta, 63, 1709-1722.
Shields, G.A., Webb, G.E., 2004, Has the REE composition of seawater changed over geologic time: Chemical Geology, 204, 103-107.
Sholkovitz, E.R., 1990, Rare earth elements in marine sediments and geochemical standards: Chemical Geology, 88, 333-347.
Siby Kurian Nath, B.N., Ramasamy, V., Naman, D., Gnaneshwar, R., Kamesh Raju, K.A., Selvaraj, K., Chen, C.T.A., 2008, Possible, detrital, diagenetic and hydrothermal sources for Holocene sediments of the Andaman backarc basin: Marine Geology, 247, 178-193.
Suárez-Vidal, F., 1987, The calcareous facies of the Alisitos Formation, evidence for an early Cretaceous tectonic calm: Ciencias Marinas, 13, 131-154.
Tardy, M., Lapierre, H., Bourdier, J., Coulon, C., Martínez, J., Otrix, E., Yta, M., Beck, C., Thery, J., 1993, Intra-oceanic settings of the western Mexico Late Jurassic-Early Cretaceous arc sequences: implications for the Pacific-Tethys geodynamic relationships during the Cretaceous: Geochimica et Cosmochimica Acta, 6, 174-185.
Taylor, S.R., McLennan, S., 1985, The Continental Crust: Its Composition and Evolution: Blackwell, Oxford, 312 pp.
Vahrenkamp, V.C., 1996, Carbon isotope stratigraphy of the Upper Kharaib and Shuaiba Formations: implications for the Lower Cretaceous evolution of the Arabian Gulf Region: American Association Petroleum Geologist Bulletin, 80, 647-62.
Van Kranendonk, M., Webb, G.E., Kamber, B.S., 2003, Geological and trace evidence for a marine sedimentary environment of deposition and biogenicity of 3.45 Ga stromatolitic carbonates in the Pilbara Craton, and support for a reducing Archaean ocean: Geobiology, 1, 91-108.
Verma, S.P., 2005, Estadística Básica para el Manejo de Datos Experimentales: Aplicación en la Geoquímica (Geoguimiometría): México, D.F., Universidad Nacional Autónoma de México, 186 pp.
Webb, G.E., Kamber, B.S., 2000, Rare earth elements in Holocene reefal microbialites: A new shallow seawater proxy: Geochimica et Cosmochimica Acta, 64, 1557-1565.
Weissert, H., Lini, A., Föllmi, K.B., Kuhn, O., 1998, Correlation of Early Cretaceous carbon isotope stratigraphy and platform drowning events: a possible link?: Palaeogeography Palaeoclimatology Palaeoecology, 137, 189-203.
Wetmore, P.H., Alsleben, H., Paterson, S.R., Ducea, M., Gehrels, G., Valencia, V., 2005, Field trip to the Northern Alisitos arc segment: ancestral Agua Blanca falt region, *in*VII International Meeting of the Peninsular Geological Society: Ensenada Baja California, México, Peninsular Geological Society 51 pp.
Wheat, C.G., Motti, M.J., Rudnicki, M., 2002, Trace elements and REE composition of a low-temperature ridge-flank hydrothermal spring: Geochimica et Cosmochimica Acta, 66, 3693-3705.
Wronkiewicz, D.J., Condie, K.C., 1990, Geochemistry and mineralogy of sediments from the Ventersdorp and Transvaal Supergroups, South Africa: cratonic evolution during the early Proterozoic: Geochimica et Cosmochimica Acta, 54, 343-354.
Zhang, J., Nozaki, Y., 1996, Rare earth elements and yttrium in seawater: ICP-MS determinations in the East Caroline, Coral Sea, and South Fiji basins of the western South Pacific Ocean: Geochimica et Cosmochimica Acta, 60, 4631-4644.

Manuscript received: december 31, 2016
Corrected manuscript received: april 20, 2017
Manuscript accepted: april 24, 2017